Available online at www.sciencedirect.com

SciVerse ScienceDirect

Ceramics International 39 (2013) 7921–7926

CERAMICS INTERNATIONAL

www.elsevier.com/locate/ceramint

Fabrication of transparent neodymium-doped yttrium aluminum garnet ceramics by high solid loading suspensions

Xiangbo Ji[a,b], Jianguo Deng[a], Bin Kang[a], Hui Huang[a,*], Xin Wang[b], Wei Jing[a], Tao Xu[a]

[a]*Institute of Chemical Materials, CAEP, Mianyang 621900, China*
[b]*School of Chemical Engineering, NUST, Nanjing 210094, China*

Received 17 January 2013; received in revised form 15 March 2013; accepted 16 March 2013
Available online 3 April 2013

Abstract

Dense neodymium-doped yttrium aluminum garnet (Nd:YAG) transparent ceramic was obtained by slip casting and solid-state reaction. The colloidal behavior of the aqueous suspensions of neodymia, yttria, and alumina mixed powders using Dispex A as dispersant was investigated. The variation in zeta potential due to pH alteration was studied. The isoelectric point (IEP) was at pH 4.5 and 4 for the specimens with and without Dispex A, respectively. The optimal dispersion conditions were achieved for the suspensions at pH 9.6 with 0.4 wt% Dispex A. The green body prepared by slip casting was vacuum sintered from 1200 °C to 1750 °C. The grain size of the sintered body increased, and the pore size decreased with increasing sintering temperature. Pore-free Nd:YAG transparent ceramic with a grain size of 5–10 μm was obtained by sintering at 1750 °C for 10 h. The in-line transmittance of the annealed specimen reached 80.8% at 1064 nm.

Keywords: A. Suspension; Nd:YAG; Solid loading; Transparent ceramic

1. Introduction

Since the first polycrystalline Nd:YAG ceramic laser pumped by the diode laser excitation system was first reported by Ikesue et al. [1,2], laser ceramics have attracted considerable attention because of their greatly improved optical quality, which have produced highly efficient laser oscillations [3–7]. Compared with single crystals, Nd:YAG laser ceramic has superior properties, such as the ease of fabrication into complicated structures and the possibility for mass production [8–10]. A high density and a uniform green body are key factors to obtaining high-quality Nd:YAG laser ceramics. Two previously reported methods are used to obtain Nd:YAG ceramic green bodies [11–13]. Dry pressing is the most common technique for creating transparent Nd:YAG ceramics. High-purity Y_2O_3, Al_2O_3, and Nd_2O_3 powders are blended, ball milled, and pressed under low pressure into required shapes, and then cold isostatically pressed under a relatively high pressure [14,15]. However, a pore-free ceramic is difficult to obtain with vacuum sintering using the press formation method because some air is always trapped in the closed micro-cavities formed by the tightly compacted particles in the green body during high-pressure formation. Nanopowder technology combined with the slip casting method is a proven effective process in the fabrication of transparent YAG ceramics because defects such as aggregates and agglomerates can be more readily managed [16,17]. However, the stoichiometry ratio is difficult to control due to the complicated process of nanopowder fabrication.

The methods of Nd:YAG ceramic fabrication reported in most papers are dry pressing and solid-state reaction sintering [5,18–20]. However, only a few papers reported the slip casting of aqueous metal oxide mixtures to produce transparent Nd:YAG [21–23]. A key point in the successful use of slip casting is achieving a well-dispersed suspension with high solid loading and low viscosity [24]. Modifying the particle surface with surfactants is necessary to achieve adequate distance between the particles in ceramic suspensions [25,26]. Both poly(acrylic acid) and ammonium polyacrylate are proven efficient dispersants in the aqueous solution of Y_2O_3, Al_2O_3, and Nd_2O_3 powders. However, the reported rheology varied with the molecular weights of the dispersants used and the statuses of the oxide powders [21,22].

*Corresponding author. Tel.: +86 028 85880792.
E-mail address: hh.caep@yahoo.cn (H. Huang).

0272-8842/$ - see front matter © 2013 Elsevier Ltd and Techna Group S.r.l. All rights reserved.
http://dx.doi.org/10.1016/j.ceramint.2013.03.054

In the present study, the aqueous slurry of commercial neodymia, yttria, and alumina mixed powders with commercial dispersant was prepared by ball milling. The effect of pH, dispersant, and solid loading on the properties of the slurry was investigated to determine a suitable stabilization method. The microstructure of the Nd:YAG ceramic prepared by slip casting with high solid loading and solid-state reaction sintering was investigated.

2. Materials and experimental procedures

High purity alumina powder (99.99%; Aladdin, China), yttria powder (99.99%; Aladdin, China), neodymia (99.95%; Aladdin, China), and Dispex A40 (40% in water; Ciba, UK) were used. The oxide powders were always weighed out in stoichiometric proportions at the (Y+Nd):Al ratio of 3:5. Neodymia was doped into the YAG at 1.0 at%. These powders were mixed in deionized water with different dispersant and solid loading concentrations. The prepared aqueous suspensions were ball milled in polyurethane jars filled with corundum milling balls for 24 h at a speed of 180 r/min.

The viscosity of the suspension with different dispersant contents was measured at room temperature in a small sample adapter at a shear rate of 13.2 s^{-1} using a Brookfield DV-II +Pro viscometer with spindle #18 (USA). The viscosity measurement of the aqueous suspensions with different solid loading and optimum dispersant concentrations was performed at shear rates ranging from 1.32 s^{-1} to 132 s^{-1}.

The zeta potentials of the diluted neodymia, yttria, and alumina mixed powder suspensions (0.01 wt%) with or without dispersant were evaluated using a JS94J potential analyzer (Powereach, China). A 0.001 M NaCl solution was prepared to maintain the ionic strength of the powder suspensions. The solution pH was adjusted by adding diluted NaOH and HCl aqueous solutions.

Solid loading suspension (70 wt%) with optimum dispersant content and 0.5 wt% tetraethoxysilane (TEOS, 99.99%; Alfa Aesar) was subsequently slip cast in plaster mold to form the green body. After the complete removal of organics by calcination at 900 °C, the green body was sintered in a vacuum furnace from 1200 °C to 1750 °C under a 1.0×10^{-3} Pa vacuum.

The Fourier transform infrared (FTIR) spectra and molecular weight of Dispex A40 were obtained using a Nicolet 6700 FTIR spectrometer (Nicolet, USA) and an Agilent gel permeation chromatograph (GPC; Agilent, USA). Morphological observations were performed with an EVO 18 scanning electron microscope (SEM; Carl Zeiss, German). Transmission measurement on polished ceramic was performed using a UV–vis and FTIR spectrometer (Lamda 35; PerkinElmer, USA).

3. Results and discussion

Fig. 1 shows the SEM micrographs of the starting alumina, yttria, and neodymia powders and the mixed powder after ball milling for 24 h. The primary alumina particles with a mean diameter of 0.4 μm were less agglomerated compared with the other powders. No clearly agglomerated particles were observed in the SEM micrographs of the yttria, but some particles about 5 μm in size were found. The neodymia powders mainly contained micrometer-sized aggregates of nanosized primary particles. The sizes of particles after ball milling decreased obviously. However, clear yttria particles with a diameter more than 1 μm were observed.

Fig. 2 shows the molecular weight distribution of the Dispex A determined by GPC using deionized water as solvent. The polyelectrolyte was quite polydisperse with an average Mw=7320. Fig. 3 shows the FTIR spectra of the Dispex A aqueous solution. The two peaks caused by the hydrogen bonding of the O–H and N–H bonds in the molecule were overlapped with a wide band from 3600 cm^{-1} to 3000 cm^{-1}. The band at 1453 cm^{-1} is attributed to the overlapping of the —COO– stretching vibration with the C–C asymmetric deformation [27]. In addition, the bands at 1324 and 1043 cm^{-1} are attributed to the skeletal C–C vibrations, and the absorption band at about 1644 cm^{-1} is attributed to the bending vibration of N–H, thereby confirming the presence of NH_4^+ [28]. Thus, Dispex A was a polycarboxylic acid ammonium with an average molecular weight of 7320.

Obtaining homogeneously dispersed suspensions with high solid loading is important to prepare high-quality ceramic parts by slip casting. In ceramic suspensions, a close correlation exists between the rheological property and the suspension structure, which depends on the zeta potential of the powders [29]. The effect of pH on the zeta potential of the powder in the slurry is shown in Fig. 4. The addition of Dispex A produced a pronounced effect on the electrokinetic behaviors of the mixed powders. The isoelectric point (IEP) is the value at which the net surface charge of a particle is zero [30]. The IEP of the mixed powder suspensions changed from pH 4.5 to 4. The particle surface is positively charged at pH < IEP and negatively charged at pH > IEP. The curve shapes of the zeta potentials for the powder with or without dispersant remained almost the same. The zeta potential absolute value increased with increasing pH at pH > IEP because of the increasing double-layer thickness and the total surface charge of the particle. The particles with dispersant exhibited a higher negative zeta potential than that of the particles without dispersant at the same pH ranging from 4.5 to 10 because of the absorption of dispersant on the powder. In this case, thermodynamic theories explain adsorption as a process that lowers the free energy of the system [31]. The Dispex A molecules contain the functional group $–COONH_4$, which dissociated into $–COO^{-1}$ when Dispex A was dissolved in the aqueous solution. The fraction dissociated or the percentage of the number of $–COO^{-1}$ to the total number of functional groups is affected by the pH value of the solution. With increasing pH, the additional [$–COO^{-1}$] resulted in well-dispersed, highly stable suspensions [32]. The absolute value of zeta potential of the powders with dispersant reached 61 at pH=9.6. The effect of the dispersant on the zeta potential was negative at pH > 10 because of the surface dissolution and hydrolysis of yttria.

Fig. 5 shows the relationship between the apparent viscosity of the alumina suspension at pH 9.6 and the additive concentration

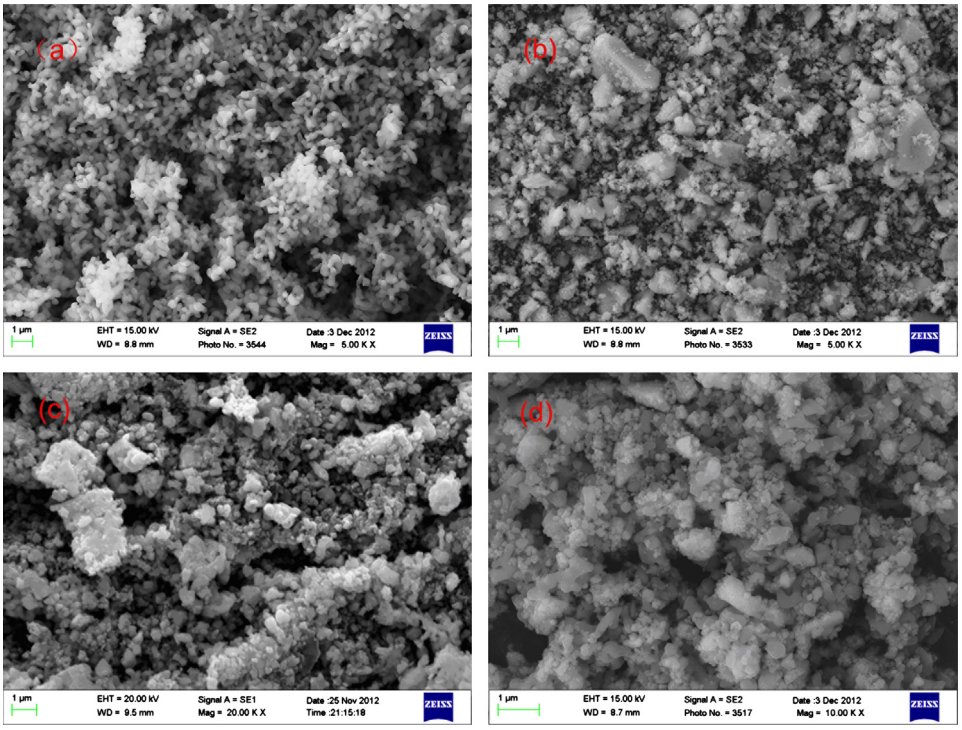

Fig. 1. SEM micrographs of the starting materials: (a) Al_2O_3, (b) Y_2O_3, (c) Nd_2O_3, and (d) ball-milled mixed powder.

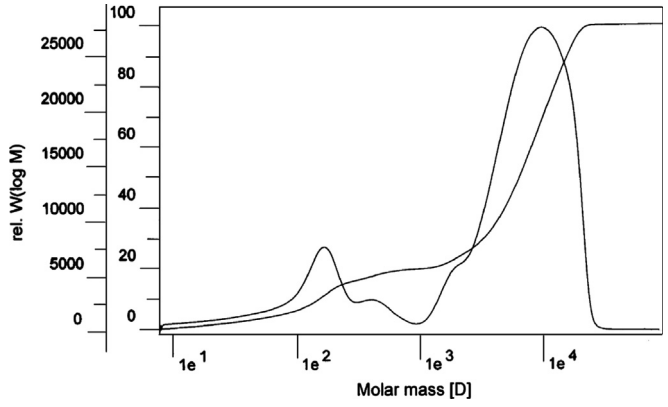

Fig. 2. Molecular weight distribution of Dispex A using deionized water as solvent.

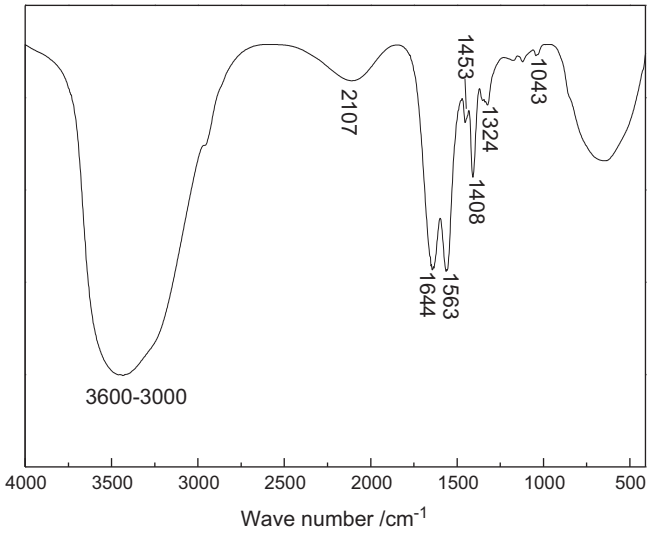

Fig. 3. FTIR spectra of Dispex A aqueous solution.

of the polymer dispersant. The apparent viscosity decreased with an increase of additive content at concentrations below 0.3 wt%. The optimum additive content for obtaining the minimum apparent viscosity ranged from 0.3 wt% to 0.4 wt%. The excessive addition of polymer dispersant (higher than 0.4 wt%) increased the apparent viscosity of the suspension. The addition of dispersant beyond the maximum coverage of the particle surface leads to an excess of dispersant in the solution. The excess dispersant exerts negative effects on the rheology by acting as a free electrolyte or forming a second adsorbed layer on the surface of particles with an opposite orientation [33,34]. The former may lead to depletion by flocculation because of the osmotic force or pressure created by the exclusion of the unadsorbed polymer chains between two approaching particles coated by the dispersant. The latter, on the other hand, may lead to repulsive electrostatic particle interactions at higher dispersant concentrations.

Fig. 6 gives the plots of apparent viscosity vs. the applied shear rate of stable suspensions with solid loading from 60 wt % to 72 wt% after milling for 24 h. The viscosity, which was high at a low shear rate, decreased with increasing shear rate. There exists an intimate relation between the particle interactions, including Brownian motion, the suspension structure, and the rheological response [35]. The fluid mechanical interactions and the interparticle forces are strongly dependent on the average separation distance between the suspended

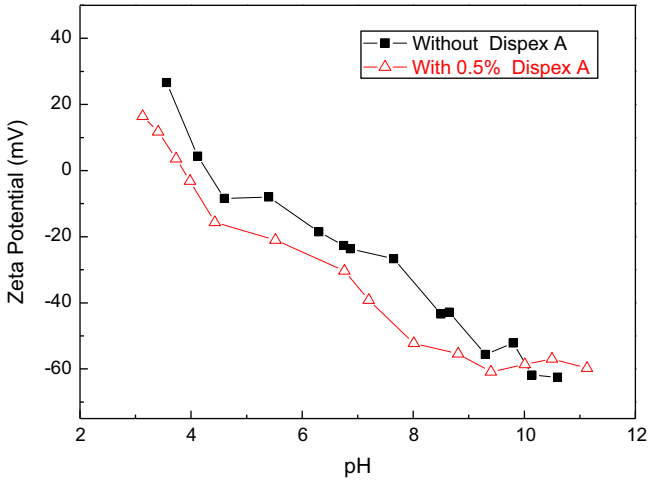

Fig. 4. Variation of zeta potential with pH for neodymia, yttria, and alumina mixed powder suspensions with and without Dispex A.

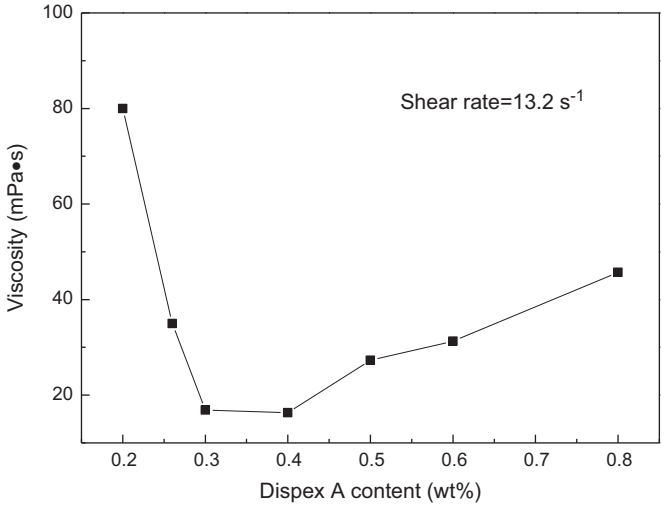

Fig. 5. Influence of Dispex A content on the viscosity of neodymia, yttria, and alumina mixed powder suspensions with 70 wt% solid loading.

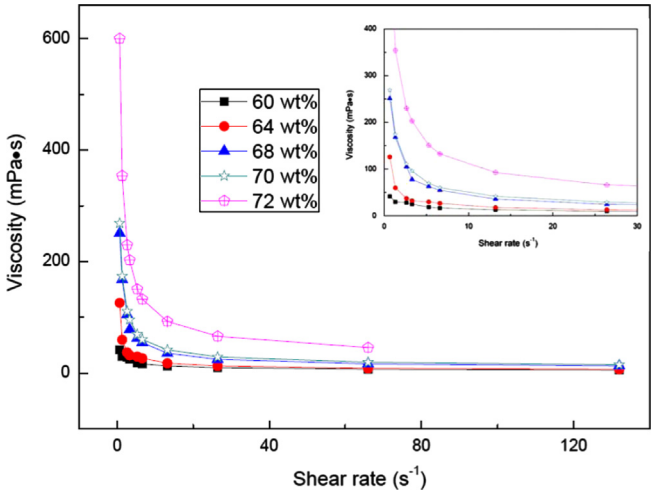

Fig. 6. Effect of solid loading on the viscosity of neodymia, yttria, and alumina mixed powder suspensions with 0.4 wt% Dispex A as dispersant.

particles [36]. These suspensions display a shear thinning behavior in steady shear because of the perturbation of the suspension structure by shear. At low shear rates, the suspension structure is close to that of equilibrium, because thermal motion dominates over the viscous forces. At higher shear rates, the viscous forces affect the suspension structure, and shear thinning occurs. The viscosity of the suspension was strongly dependent on the solids loading at low shear rates. The properties of the aggregating suspension change drastically at a certain critical particle concentration (> 72 wt%), at which the average separation distance between the particles tends to zero and the particles pack together, making flow impossible.

The 70 wt% solid loading suspension with 0.4 wt% dispersant content and 0.5 wt% TEOS was slip cast in a plaster mold to form the green body. The green body was air-calcined at 900 °C to remove the organics and then sintered in the vacuum furnace from 1200 °C to 1750 °C. Fig. 7 shows the microstructure of the fractured surfaces of the Nd:YAG ceramic and Fig. 8 shows the relative density vs. sintered temperature. The relative density slowly increased with increasing sintered temperature. The sintered body densified to over 97% relative density at 1700 °C for 5 h. The specimen sintered at the temperature less than 1700 °C is opaque because of its higher porosity. Furthermore, the figure indicated that the grain size increased and the pore size decreased with increasing sintering temperature. The specimen sintered at 1700 °C was cloudy because of numerous pores captured in the grain boundaries. Grain growth is an important process in removing the final pores and in obtaining Nd:YAG transparent ceramics with high density. A dense, pore-free microstructure was observed at 1750 °C for 10 h and the average grain size was about 5–10 μm. Fig. 9 shows the room temperature optical transmittance of a 1.0 at% Nd:YAG sample with 2.1 mm in thickness. A photo of annealed Nd:YAG ceramics in air is shown in the inset of the figure. The in-line transmittance of annealed sample has reached 80.8% at 1064 nm, indicating good optical quality.

4. Conclusion

Neodymia, yttria, and alumina mixed powder aqueous suspensions were prepared by using Dispex A as dispersants. It was found that Dispex A enhanced dispersion and stability of the suspensions. The measurements of zeta potential vs. pH values and suspension viscosity as a function of dispersant concentration indicated that the optimum additive content for obtaining the minimum apparent viscosity ranged from 0.3 wt % to 0.4 wt% at pH=9.6. The effects of solid loading on viscosity of the suspensions prepared with 0.4 wt% dispersant were also investigated. The viscosity of the suspension was strongly dependent on the solids loading at low shear rate. These suspensions with solid loading from 60 wt% to 72 wt% display a shear thinning behavior. The Nd:YAG green body was prepared by slip casting with 70 wt% solid loading and 0.4 wt% Dispex A. Dense Nd:YAG transparent ceramic with a

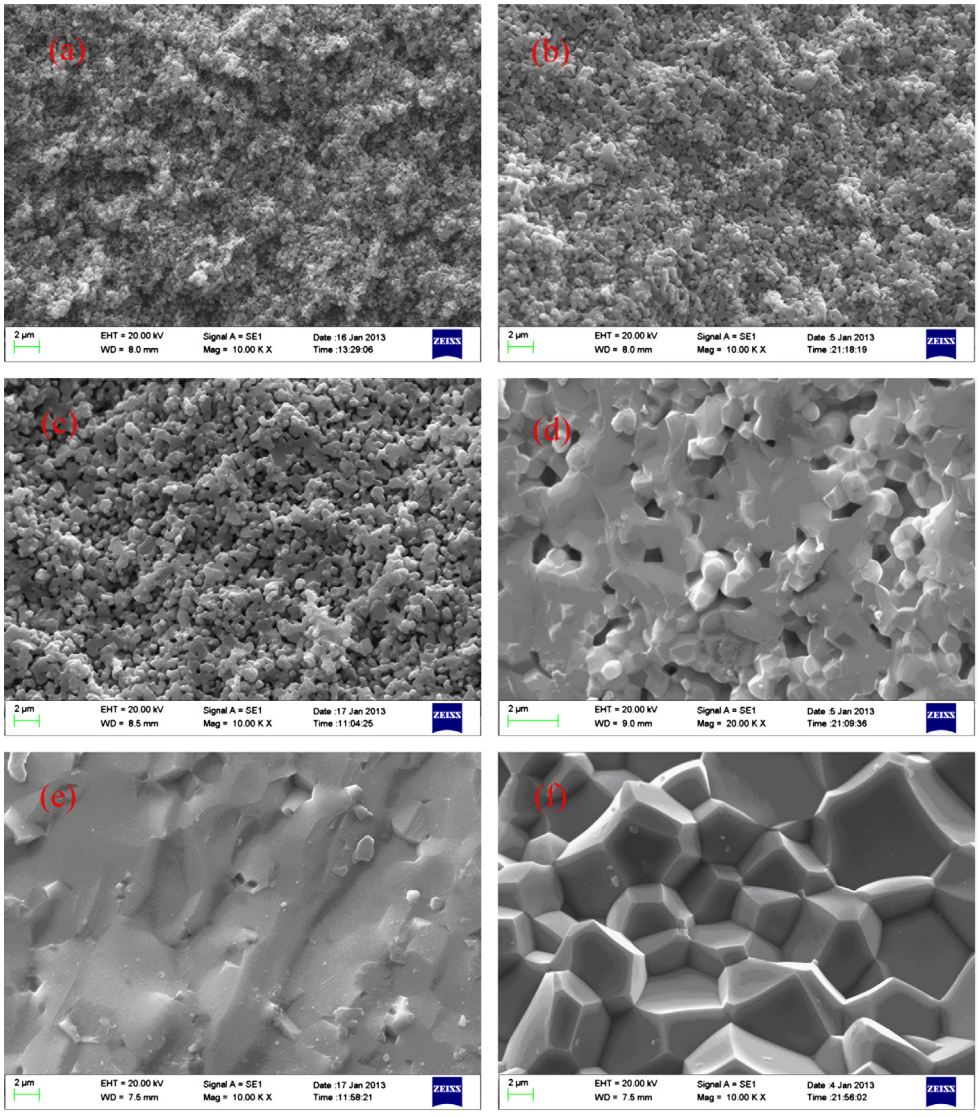

Fig. 7. SEM micrographs of the fractured surfaces of Nd:YAG ceramic sintered at (a) 1200 °C for 5 h, (b) 1400 °C for 5 h, (c) 1500 °C for 5 h, (d) 1600 °C for 5 h, (e) 1700 °C for 5 h, and (f) 1750 °C for 10 h.

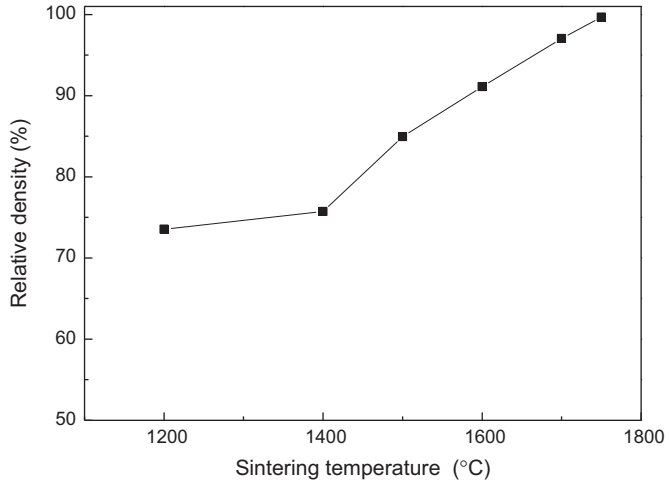

Fig. 8. Relative density vs. temperature for the Nd:YAG ceramics sintered for 5 h.

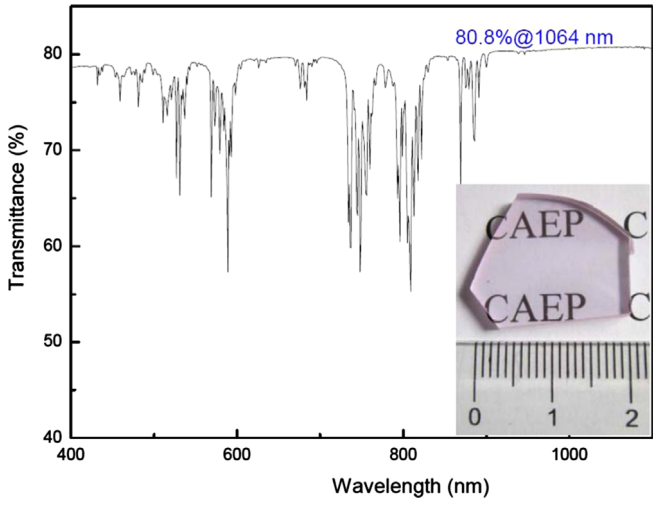

Fig. 9. Optical transmittance spectra and photograph (inset image) of 1 at% doped Nd:YAG ceramics (2.1 mm thick) after annealing process.

grain size of 5–10 μm was obtained via the solid-state reaction and vacuum sintering at 1750 °C for 10 h.

Acknowledgments

The authors are grateful for the support of this work by the Key Laboratory of Science and Technology on High Energy Laser, CAEP.

References

[1] A. Ikesue, I. Furusato, K. Kamata, Fabrication of polycrystalline transparent YAG ceramics by a solid-state reaction method, Journal of the American Ceramic Society 78 (1) (1995) 225–228.
[2] A. Ikesue, T. Kinoshita, K. Kamata, K. Yoshida, Fabrication and optical-properties of high-performance polycrystalline Nd:YAG ceramics for solid state lasers, Journal of the American Ceramic Society 78 (4) (1995) 1033–1040.
[3] H. Yagi, T. Yanagitani, K. Takaichi, K. Ueda, A. Kaminskii, Characterizations and laser performances of highly transparent Nd^{3+}:$Y_3Al_5O_{12}$ laser ceramics, Optical Materials 29 (10) (2007) 1258–1262.
[4] J. Lu, M. Prabhu, K. Ueda, H. Yagi, T. Yanagitani, A. Kudryashov, A. A. Kaminskii, Potential of ceramic YAG lasers, Laser Physics 11 (10) (2001) 1053–1057.
[5] W. Liu, J. Li, B. Jiang, D. Zhang, Y. Pan, 2.44 kW laser output of Nd: YAG ceramic slab fabricated by a solid-state reactive sintering, Journal of Alloys and Compounds 538 (2012) 258–261.
[6] J. Lu, M. Prabhu, J. Xu, Highly efficient 2% Nd:yttrium aluminum garnet ceramic laser, Applied Physics Letters, 77, 3707–3709.
[7] J. Zhou, W. Zhang, T. Huang, L. Wang, J. Li, W. Liu, B. Jiang, Y. Pan, J. Guo, Optical properties of Er,Yb co-doped YAG transparent ceramics, Ceramics International 37 (2) (2011) 513–519.
[8] A. Ikesue, Y.L. Aung, Synthesis and performance of advanced ceramic lasers, Journal of the American Ceramic Society 89 (6) (2006) 1936–1944.
[9] J. Li, Y. Wu, Y. Pan, W. Liu, L. Huang, J. Guo, Laminar-structured YAGNd:YAGYAG transparent ceramics for solid-state lasers, International Journal of Applied Ceramic Technology 5 (4) (2008) 360–364.
[10] X. Ba, J. Li, Y. Zeng, Y. Pan, B. Jiang, W. Liu, W. Liang, J. Liu, J. Guo, Transparent $Y_3Al_5O_{12}$ ceramics produced by an aqueous tape casting method, Ceramics International 39 (4) (2013) 4639–4643.
[11] A. Ikesue, T. Kinoshita, K. Kamata, Fabricaton and optical properties of high-performance polycrystalline Nd:YAG ceramics for solid-state lasers, Journal of the American Ceramic Society 78 (4) (1995) 1033–1020.
[12] W. Liu, J. Li, B. Jiang, D. Zhang, Y. Pan, Effect of La_2O_3 on microstructures and laser properties of Nd:YAG ceramics, Journal of Alloys and Compounds 512 (1) (2012) 1–4.
[13] A. Ikesue, K. Kamata, K. Yoshida, Synthesis of Nd^{3+},Cr^{3+}-codoped YAG ceramics for high-efficiency solid-state lasers, Journal of the American Ceramic Society 78 (9) (1995) 2545–2547.
[14] H. Yang, J. Zhang, X. Qin, D. Luo, J. Ma, D. Tang, H. Chen, D. Shen, Q. Zhang, T. Stefanik, Polycrystalline Ho:YAG transparent ceramics for eye-safe solid state laser applications, Journal of the American Ceramic Society 95 (1) (2012) 52–55.
[15] H. Yang, X. Qin, J. Zhang, J. Ma, D. Tang, S. Wang, Q. Zhang, The effect of MgO and SiO_2 codoping on the properties of Nd:YAG transparent ceramic, Optical Materials 34 (6) (2012) 940–943.
[16] J.-h. Liu, X.-q. Piao, L.-p. Lu, X.-x. Guan, Y.-c. Wan, Preparation of transparent laser ceramics Er:YAG by carbonate co-precipitation method, Journal of Synthetic Crystals 33 (3) (2004) 407–410.
[17] H. Yagi, K. Takaichi, K.-i. Ueda, T. Yanagitani, A.A. Kaminskii, Influence of annealing conditions on the optical properties of chromium-doped ceramic $Y_3Al_5O_{12}$, Optical Materials 29 (4) (2006) 392–396.
[18] A. Ikesue, Y. Aung, Synthesis and performance of advanced ceramic lasers, Journal of the American Ceramic Society 89 (2006) 1936–1944.
[19] W. Zhang, T. Lu, N. Wei, B. Ma, F. Li, Z. Lu, J. Qi, Effect of annealing on the optical properties of Nd:YAG transparent ceramics, Optical Materials 34 (4) (2012) 685–690.
[20] F. Tang, Y. Cao, J. Huang, H. Liu, W. Guo, W. Wang, V.B. Kravchenko, Fabrication and laser behavior of composite Yb:YAG ceramic, Journal of the American Ceramic Society 95 (1) (2012) 56–69.
[21] W. Guo, Y. Cao, Q. Huang, J. Li, J. Huang, Z. Huang, F. Tang, Fabrication and laser behaviors of Nd:YAG ceramic microchips, Journal of the European Ceramic Society 31 (13) (2011) 2241–2246.
[22] Y. Lv, W. Zhang, J. Tan, Y. Sang, H. Qin, J. Hu, L. Tong, H. Liu, J. Wang, R.I. Boughton, Dispersion of concentrated aqueous neodymia–yttria–alumina mixture with ammonium poly(acrylic acid) as dispersant, Journal of Alloys and Compounds 509 (6) (2011) 3122–3127.
[23] K. Appiagyei, G. Messing, J. Dumm, Aqueous slip casting of transparent yttrium aluminum garnet (YAG) ceramics, Ceramics International 34 (5) (2008) 1309–1313.
[24] c.R. Evanko, D.A. Dzombak, J.W. Novak Jr., Influence of surfactant addition on the stability of concentrated alumina dispersions in water, Colloids and Surfaces 110 (1996) 219–233.
[25] F. Boschini, A. Rulmont, R. Cloots, R. Moreno, Colloidal stability of aqueous suspensions of barium zirconate, Journal of the European Ceramic Society 25 (13) (2005) 3195–3201.
[26] A. Zingg, F. Winnefeld, L. Holzer, J. Pakusch, S. Becker, L. Gauckler, Adsorption of polyelectrolytes and its influence on the rheology, zeta potential, and microstructure of various cement and hydrate phases, Journal of Colloid and Interface Science 323 (2) (2008) 301–312.
[27] C. Rödel, M. Müller, M. Glorius, A. Potthoff, A. Michaelis, Effect of varied powder processing routes on the stabilizing performance and coordination type of polyacrylate in alumina suspensions, Journal of the European Ceramic Society 32 (2) (2012) 363–370.
[28] K. Cai, M. Ode, H. Murakami, Influence of polyelectrolyte dispersants on the surface chemical properties of aluminum in aqueous suspension, Colloids and Surfaces A: Physicochemical and Engineering Aspects 284–285 (2006) 458–463.
[29] S.B. Johnson, G.V. Franks, P.J. Scales, D.V. Boger, T.W. Healy, Surface chemistry–rheology relationships in concentrated mineral suspensions, International Journal of Mineral Processing 58 (2000) 267–304.
[30] F. Shojai, A.B.A. Pettersson, T. Mantyla, J.B. Rosenholm, Electrostatic and electrosteric stabilization of aqueous slips of 3Y–ZrO_2 powder, Journal of the European Ceramic Society 20 (2000) 277–283.
[31] J.-F. Lambert, Adsorption and polymerization of amino acids on mineral surfaces: a review, Origins of Life and Evolution of Biospheres 38 (3) (2008) 211–242.
[32] M.C.B. Lopez, B. Rand, F.L. Riley, Polymeric stabilisation of aqueous suspensions of barium titanate. Part I: Effect of pH, Journal of the European Ceramic Society 20 (2000) 1579–1586.
[33] N. Traiphol, R. Suntako, K. Chanthornthip, Roles of polymeric dispersant charge density on lead zirconate titanate aqueous processing, Ceramics International 36 (7) (2010) 2147–2153.
[34] K.-L. Ying, T.-E. Hsieh, Y.-F. Hsieh, Colloidal dispersion of nano-scale ZnO powders using amphibious and anionic polyelectrolytes, Ceramics International 35 (3) (2009) 1165–1171.
[35] W.M. Sigmund, N.S. Bell, L. Bergstrom, Novel powder-processing methods for advanced ceramics, Journal of the American Ceramic Society 83 (7) (2000) 1557–1574.
[36] B.H.G.E. Tamjid, Rheology and colloidal structure of silver nanoparticles dispersed in diethylene glycol, Powder Technology 197 (2010) 49–53.